RESEARCH ARTICLE | JUNE 12 2024

Ultrafast supercontinuum sculpting for two-photon spectroscopy and microscopy of ratiometric fluorescent indicators

Artem S. Chebotarev ; Roman I. Raevsky ; Georgy N. Linovsky ; Alexander I. Kostyuk ; Vsevolod V. Belousov ; Andrei B. Fedotov; Dmitry S. Bilan ; Aleksandr A. Lanin

Appl. Phys. Lett. 124, 243704 (2024)
https://doi.org/10.1063/5.0197580

Applied Physics Letters ARTICLE pubs.aip.org/aip/apl

Ultrafast supercontinuum sculpting for two-photon spectroscopy and microscopy of ratiometric fluorescent indicators

Cite as: Appl. Phys. Lett. **124**, 243704 (2024); doi: 10.1063/5.0197580
Submitted: 13 January 2024 · Accepted: 3 June 2024 ·
Published Online: 12 June 2024

View Online Export Citation CrossMark

Artem S. Chebotarev,[1] Roman I. Raevsky,[2,3] Georgy N. Linovsky,[1] Alexander I. Kostyuk,[2,3] Vsevolod V. Belousov,[2,3,4] Andrei B. Fedotov,[1] Dmitry S. Bilan,[2,3] and Aleksandr A. Lanin[1,a)]

AFFILIATIONS

[1]Physics Department, M.V. Lomonosov Moscow State University, 111992 Moscow, Russia
[2]M.M. Shemyakin and Yu.A. Ovchinnikov Institute of Bioorganic Chemistry, Russian Academy of Science, 117997 Moscow, Russia
[3]Pirogov Russian National Research Medical University, 117997 Moscow, Russia
[4]Federal Center of Brain Research and Neurotechnologies, Federal Medical-Biological Agency, 119330 Moscow, Russia

[a)]**Author to whom correspondence should be addressed:** lanin@physics.msu.ru

ABSTRACT

We present a compact laser system for quantitative two-photon excitation spectra measurements and ratiometric two-photon imaging of fluorescent protein indicators. The fundamental of the system is a short segment of photonic crystal fiber (PCF), which supports a nonlinear transformation of low-power ultrashort pulses by preserving temporal coherence, and this generates an ultrafast almost octave-spanning supercontinuum (SC). Accurate sculpting of the SC by its amplitude and phase modulation provides implementation of the spectroscopic and microscopic modalities. The spectroscopic one was exhibited by two-photon action cross section spectra measuring for the genetically encoded fluorescent sensing proteins of the vital biochemical parameters: acidity (SypHer3s), concentration of hydrogen peroxide (HyPer3 and HyPer7), redox status of NADH and glutathione (RexYFP and Grx1-roGFP2), hypohalous acids and their derivatives (Hypocrates). For the microscopy, we investigated and optimized the intensity pump pulse profiles under the high numerical objective by dispersion scan technique. We conducted real-time monitoring of the dynamics of hydrogen peroxide in HeLa cells with subcellular spatial resolution by means of ratiometric two-photon imaging of Hyper7 sensors. The presented hybrid laser system provides an ideal optical toolbox in order to develop ratiometric fluorescent sensors, which can be visualized *in vivo* using two-photon microscopy.

Redox reactions in living animals, mediated by numerous biological molecules, contribute greatly to intra- and inter-cell signaling processes involving transcription, proliferation, metabolism regulation, regeneration, as well as tissue damage.[1–9] To real-time monitoring of the specific regulators in organisms, genetically encoded fluorescent indicators (GEFIs), which fused to proteins of interest, have provided significant advances.[10–13] Two- and three-photon excitation fluorescence (2PEF and 3PEF) microscopy grant the high contrast imaging with subcellular resolution of fluorescent agents from the deep layers of scattering tissue, but its realization faces difficulties with continuous ratiometric readout.[14–19] Analysis of two-photon absorption (TPA) cross section spectra of fluorescent indicators reveals the hyperpolarization of used chromophore and the static electric field environment, which could be crucial to design bright, highly sensitive sensors for fluorescent microscopy.[20–24] For this purpose, expansive and complicated laser systems have been developed involving optical parametric amplifiers,[21,22,25,26] tunable powerful laser generators,[15,17,27] and synchronously pumped optical parametric oscillators.[23,28] Broadband, spectral, and temporal tuned ultrashort pulses generated in various types of photonic crystal fibers (PCFs) are extensively used in multimodal nonlinear imaging.[29–36] Studies have shown that a compact laser system consisting of an ultrafast Yb-fiber oscillator, an all-normal dispersion photonic crystal fiber, and a pair of chirped mirrors can generate pulses in the 720–930 nm range with a duration of 14-fs for two-photon microscopy.[36]

In this work, we present a compact laser optical toolbox integrated with a dual-channel 2PEF microscopy for the investigation of nonlinear optical properties of fluorescent indicators and its potential for ratiometric two-photon imaging. We provided accurate nonlinear transformation of low-power pulses in a photonic crystal fiber (PCF) to an ultrashort sub-octave-spanning supercontinuum (SC) generation and its amplitude and phase tuning to produce an appropriate source

for both TPA spectra measurements and ratiometric dual-channel 2PEF imaging. Such a laser source was exploited for quantitative TPA spectra measurements of a palette of redox and metabolism cell status sensors, including indicators of hydrogen peroxide (H_2O_2), HyPer3[37] and HyPer7,[38] the ratios of the oxidized and reduced forms of nicotinamide adenine dinucleotide and glutathione (NAD+/NADH and GSSH/GSH), RexYFP[39] and Grx1-roGFP2,[40,41] and hypohalous acids and intracellular pH-level, Hypocrates[42] and SypHer3s.[43] Imaging capabilities of the apparatus were shown through the recording of the time lapses of H_2O_2 dynamics in HeLa cells by means of the ratiometric 2PEF microscopy of HyPer7 sensor.

The main principle of the functioning of most GEFIs is based on the fact that the analyte molecule interacts with the sensory domain and causes conformational rearrangements, which are transmitted to the fluorescent part. As a result, changes in the structure of the chromophore microenvironment are expressed in change of the surrounding electric field near the chromophore and its one- and two-photon excitation spectra modification [Figs. 1(a) and 1(b)]. We studied in the two-photon excitation mode the spectral properties of indicators based on circular permutant of yellow fluorescent protein (cpYFP) that was integrated into the structure of bacterial sensor proteins (OxyR in HyPer family probes, NemR in Hypocrates, T-Rex in RexYFP) as well as the so-called redox-sensitive fluorescent proteins using the example of the most popular representative Grx1-roGFP2,[41] which are characterized by the presence of a pair of redox-active cysteines on adjacent beta sheets of the GFP barrel structure.

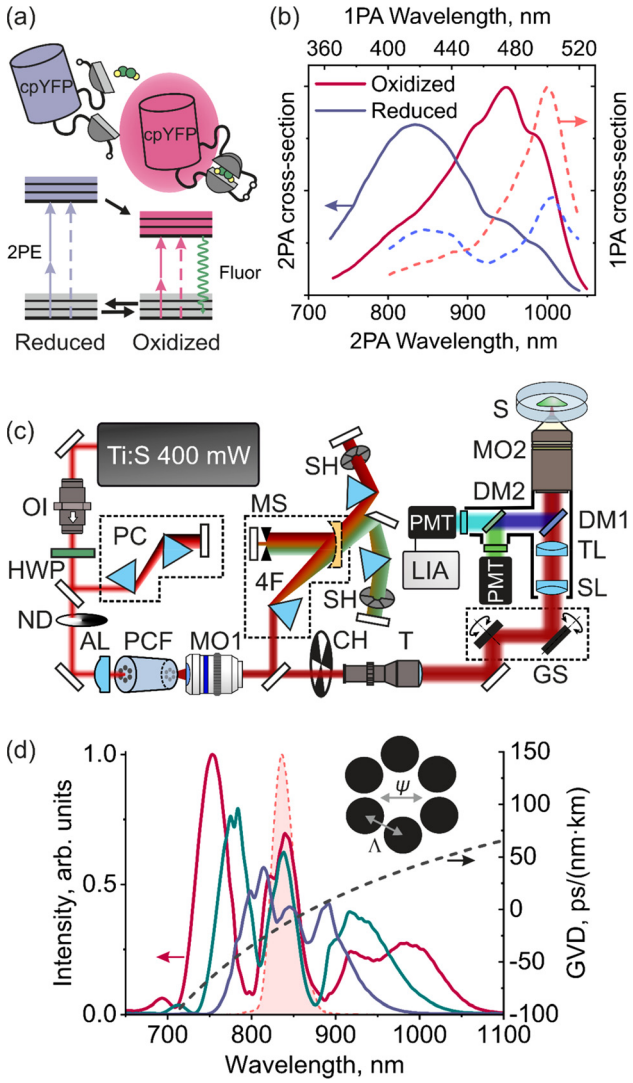

FIG. 1. (a) The diagram of a cpYFP-based sensor. (b) One- and two-photon (dashed and solid lines) excitation spectra of ratiometric HyPer sensor in reduced (pink lines) and oxidized by H_2O_2 (navy lines) forms. (c) Optical scheme: Ti:S, Ti:S laser; OI, optical isolator; HWP, half-wavelength plate; PC, prism compressor; AL, aspheric lens; MO, microscopic objective; 4F, 4f-imaging system; MS, motorized slit, SH, shutter; CH, optical chopper; GS, galvano-scanner; SL: scan lens; TL: tube lense; DM, dichroic mirror; PMT, photomultiplier tube; LIA, lock-in amplifier; S, sample. (d) The SC spectra from the PCF at the pump power of 50 mW (blue), 80 mW (cyan), and 110 mW (red); the pump pulse spectrum is shown by the dashed pink line. Calculated GVD of the PCF (black dashed line).

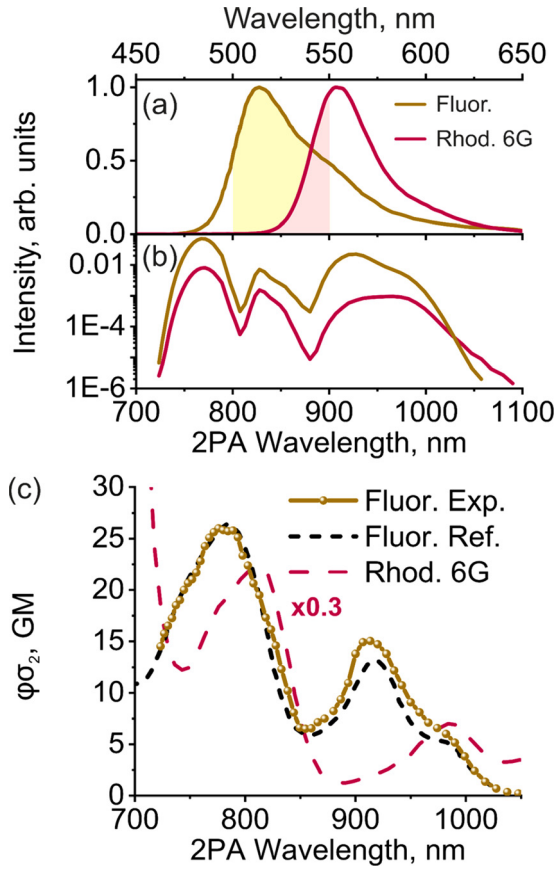

FIG. 2. (a) Two-photon excited emission spectra of rhodamine 6G (red line) and fluorescein (yellow line). The shaded area shows the detection region of 500–550 nm. (b) The PMT signal $Sr(\lambda)$ of rhodamine 6G (red line) and $S_s(\lambda)$ of fluorescein (yellow line) excited by the amplitude modulated SC. (c) Comparison of the measured $\varphi\sigma_2(\lambda)$-spectrum of fluorescein (yellow line) with the one provided by de Reguardati *et al.*[26] (black short dashed line) and the referenced rhodamine 6G spectrum (red dashed line).

The main laser source of the hybrid imaging and spectroscopic system [Fig. 1(c)] is a compact ultrafast titanium:sapphire (Ti:S) laser, which provides 50-fs-pulses with an energy up to 5 nJ in the range of 770–880 nm (Avesta-project). The most bright and coherent SC spanning from 700 to 1100 nm [Fig. 1(c)] was generated in the 13-mm-length PCF, having a honeycomb cladding structure with a hole diameter of $\psi = 2.4\,\mu$m and a pitch of $\Lambda = 2.7\,\mu$m [inset in Fig. 1(c)], when the pump pulses at 840 nm fall in the area of small positive group velocity dispersion (GVD).[44] We installed a supporting SF14-glass prism compressor after the optical isolator to conserve the high peak power of the pulses on the PCF input tip. To provide high spatial resolution multiphoton microscopy with such a fiber-based laser source, the SC was collimated from the PCF by a low aberration in IR region objective LCPlanN 50x/0.65, Olympus. In order to produce a bright nonlinear response via such a source, we measured the beam profile and quality factor M2 (~1.2 at the central wavelengths of 780 and 940 nm), pulse width (less than 70 fs), and polarization extinction ratio (more than 15 dB) of the SC (Figs. S1 and S2). Details are presented in the supplementary material.

Furthermore, the optical scheme branched out to spectroscopic and microscopic setups using a flip mirror. To record TPA cross section spectra, we implemented an amplitude modulation of the SC spectrum in a 4f optical imaging system with spectrum decomposition by a pair of SF11-glass prisms. A slit on a motorized slider was placed in front of the back mirror for smooth tuning of the central wavelength of the 12-nm-bandwidth pulses with a power up to 5 mW and duration about 200 fs in the range of 690–1100 nm. The narrowband pulses were focused into solution by a high-aperture objective XLUMPlanFLN 20× NA1.00. The electrical signal produced by a photomultiplier tube (PMT) was amplified by a lock-in detector with a time constant of 300 ms. The full TPA cross section spectrum recording for one sample took ~1 min.

The brightness of fluorescence agents under two-photon excitation is defined by the two-photon action cross section $\varphi\sigma_2$, where φ is the quantum yield, and σ_2 is the TPA cross section. Implemented herein method of the $\varphi\sigma_2$-measurements is based on the comparison of nonlinear signals produced by the investigated sample $S_s(\lambda)$ and well-known reference dye $Sr(\lambda)$ on each central wavelength λ at the same conditions, which reduces uncertainty related to the light intensity and detector spectral sensitivity measurements.[25] The absolute values of $\varphi\sigma_2$-spectrum can be calculated by $\varphi_s\sigma_{2s}(\lambda) = \kappa(\lambda)\varphi_r\sigma_{2r}(\lambda)$, where the coefficient $\kappa(\lambda) = S_s(\lambda)C_r\int F_r(\Lambda)d\Lambda / Sr(\lambda)C_s\int F_s(\Lambda)d\Lambda$ is measurable in experiment, and $\varphi_r\sigma_{2r}(\lambda)$ is provided by the reference. In detail, $S(\lambda)$ is the PMT detected signal, C is the concentration, and $F(\Lambda)$ is the emission spectrum. The indexes s and r correspond to the investigated protein and reference dye.

The apparatus was tested and calibrated on dyes of rhodamine 6G and fluorescein, which were given as the reference dye and the measurable sample having a well-known $\varphi\sigma_2(\lambda)$-spectra.[26] Its emission spectra $F_r(\lambda)$ and $F_s(\lambda)$ had acceptable intersection under two-photon excitation [Fig. 2(a)]. Rhodamine 6G and fluorescein were dissolved in ethanol and pH 11.0 water at concentrations of $C_r = 90\,\mu$M and $C_s = 210\,\mu$M, respectively. We provided the sequential measurements of the reference and tested dye solutions [Fig. 2(b)] with two or three different SC spectra [Fig. 1(d)] due to overlay regions where SC spectral density drops and to obtain $\kappa(\lambda)$ in the range of 680–1100 nm (Fig. S3). Producing the $\kappa(\lambda)$ and independently knowing $\varphi_r\sigma_{2r}(\lambda)$ of rhodamine 6G allows us to reconstruct the $\varphi\sigma_2(\lambda)$-spectrum of fluorescein with high accuracy [Fig. 2(c)] that validates the proposed approach. Due to normalization of the nonlinear signal to $\varphi\sigma_2 C$, we can estimate the limit of detection for our system as ~1 μM GM.

To explore suitability of the PCF-based laser source for the two-photon ratiometric microscopy, we built up an inverted laser scanning microscope consisting of galvano mirrors, scan and tube lenses, and

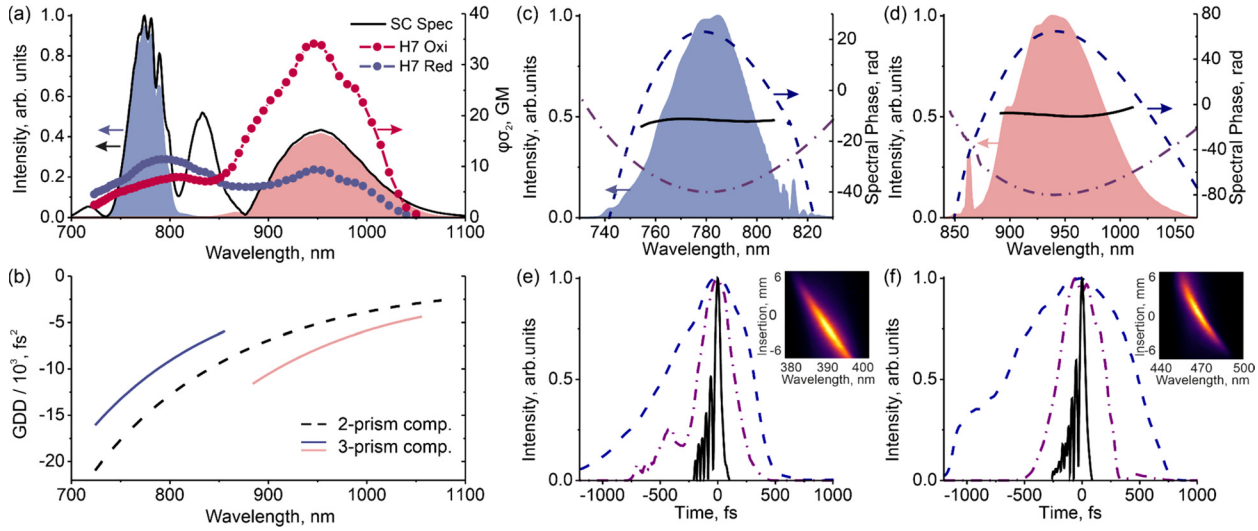

FIG. 3. (a) The SC spectrum (black dashed line) with the 80-mW pump pulse and the selected spectral features for two-color ratiometric microscopy (blue and red shaded areas) is overlaid on the TPA spectra of the reduced (blue line) and oxidized (red line) forms of HyPer7. (b) The calculated GVDs of the optimal two- and three-prism compressors (dashed and solid lines) for the microscope. (c)–(f) Spectral power densities [shaded areas in (c) and (d)], spectral phases [lines in (c) and (d)], and intensity envelopes (e) and (f) of the pulses after the IR collimating objective (purple dash-dotted lines), three-prism compressor (blue dashed lines), and on the sample (black solid lines). The d-scan maps of the pulses on the sample are shown in insets.

the same objective XLUMPlanFLN. We optimized the optical elements to deliver laser beams to sample in the wide spectral region without distortions. The detection of 2PE fluorescence in the range of 500–550 nm and second harmonic (SH) radiation below the 500 nm was produced by two PMTs in the backward direction. Image quality tuning was carried out by visualizing well-calibrated 500-nm-diameter fluorescent beads L9904 (Sigma-Aldrich) in agarose gel. The transverse and axial resolution of the 2PEF microscopy was about 500 nm and 1.9 μm at the wavelengths of 780 and 940 nm (Fig. S2), respectively.

The SC generated in the short piece of PCF predominantly due to self-phase modulation produces two pronounced spectral features at the central wavelengths of 780 and 940 nm, which are ideally suited for the selective interrogation of the reduced/oxidized protein forms in mixture [Fig. 3(a)]. These sub-pulses retain short durations due to low group delay dispersion (GDD) of the fiber. It was approved by SHG FROG measurements, giving 46 fs and 62 fs at 780 and 940 nm (Fig. S2). However, the large amount of optical elements installed in the optical path spreads the pulses to widths of ~2 ps. Solely the collimating IR objective introduces the linear $\varphi^{(2)}$ and nonlinear $\varphi^{(3)}$ chirps at 780 and 940 nm, respectively, measuring $(3.0 \pm 0.2)\times10^3$ and $(3.8 \pm 0.8)\times10^3$ fs^3 for linear chirps and $(2.2 \pm 0.1)\times10^3$ fs^2 and $(2.4 \pm 0.8)\times10^3$ fs^3 for nonlinear chirps, which spreads the pulses to 330 and 430 fs [Figs. 3(e) and 3(f)]. Single prism-pair compressor does not allow enough degrees of freedom to phase compensation in such a broad spectral region. For this purpose, we used a recently developed three-prisms compressor providing induction of negative GDD to the blue and red spectral parts of SC independently [Fig. 3(b)].[45] Quite important, the insertion of two shutters into the optical pathways of such a compressor enables it to alternate the excitation by the blue and red pulses [Fig. 1(c)]. The shutters were synchronized with the recording of two-photon microscopy frames. The optimal SF11-glass prism spacing was obtained on maximizing the SH signal generated in a BBO crystal under the microscope. The compressor arm lengths were 41 and 68 cm for the pulses at 780 and 940 nm, which result in negative chirps $\varphi^{(2)} = -(7.9 \pm 0.6) \times 10^3$ fs^2, $\varphi^{(3)} = -(24 \pm 4) \times 10^3$ fs^3, and $\varphi^{(2)} = -(6.1 \pm 0.3) \times 10^3$ fs^2, $\varphi^{(3)} = -(20 \pm 3)\times10^3$ fs^3 and durations of 760 and 1150 fs for the pulses in the entrance of the microscope [Figs. 3(c)–3(f)].

To better understand the pulse structures on the sample, a dispersion scanning (d-scan) technique was implemented.[46,47] It does not require subsequent splitting and combining of broadband pulses, assembly of an optical delay line, but just recording the spectra of SH radiation generated under smooth dispersion tuning. Therefore, the d-scan method is an excellent approach for the intensity envelope measurements of a broadband pulse on the sample surface below a high aperture objective in multiphoton microscopes equipped with a chirp compensation unit. In our case, the sample was replaced by the 20-μm-thickn BBO crystal; a glare of SH radiation was detected by a compact spectrometer, and the dispersion scanning was introduced by a motorized prism in the three-prism compressor.

Direct pulse measurements under the objective show that the envelope profiles are strongly affected by the uncompensated third order dispersion (TOD) $\varphi^{(3)}$ manifested in the d-scan maps as inclined lines [insets of Figs. 3(e) and 3(f)]. Spectral phase reconstruction gives near-zero GDD and large enough TOD of $-(16 \pm 3)\times10^3$ fs^3 and $-(15 \pm 3)\times10^3$ fs^3 for the pulses at 780 and 940 nm on the sample, which translates to the oscillatory fronts of the pulses and durations of 53 and 57 fs. As seen, the TOD is partially compensated, because different optical glasses, which are used to make achromatic optics, have material dispersion properties of $\varphi^{(3)}/\varphi^{(2)} \approx 0.8$–$1.5$ fs in the near IR region, but prism compressors provide a nearby relation of $\varphi^{(3)}/\varphi^{(2)} \approx 2.5$–$3.5$ fs with negative $\varphi^{(2)}$. Therefore, the whole GVD of conventional multiphoton microscope optical system, which lies near 10^4 fs^2, should be compensated by a diffraction grating prism (grism) compressor[48] or spatial light modulator[32] to even out the nonlinear chirp and intensity envelope distortion.

On the developed spectroscopic system, we measured TPA spectra of the indicators HyPer3, HyPer7, Grx1-roGFP2, RexYFP, Hypocrates, and SypHer3s, dissolving them in the appropriate buffers with concentrations of $C_s = 50\,\mu$M. Some of GEFIs exhibit sensitivity to pH changes and require an appropriate control probe to acidity monitoring, for example, using SypHer3s. Emission spectra of the proteins under two-photon excitation at 940 nm are close to each other and to the base protein cpYFP [Fig. 4(a)]. Furthermore, we measured the one- and two-photon absorption (OPA and TPA) spectra of the

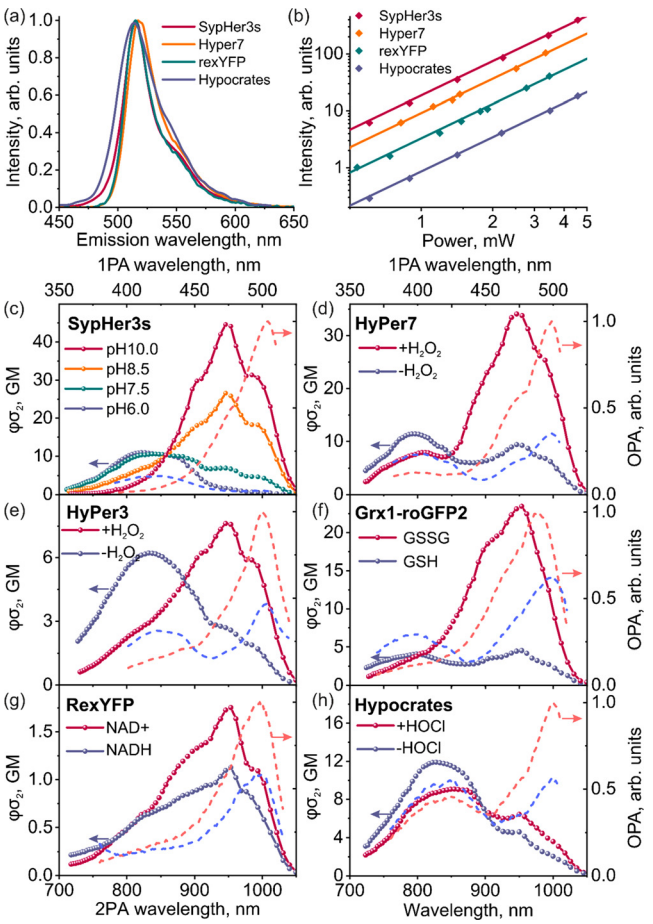

FIG. 4. Two-photon excited emission spectra (a) and IR power dependences of 2PEF signals (b) of the GEFIs. Lines show quadratic power dependences. (c)–(h) OPA (dashed lines) and TPA (solid lines) spectra of the oxidized (red lines) and reduced (blue lines) forms of SypHer3s (c), HyPer7 (d), HyPer3 (e), Grx1-roGFP2 (f), RexYFP (g), and Hypocrates (h).

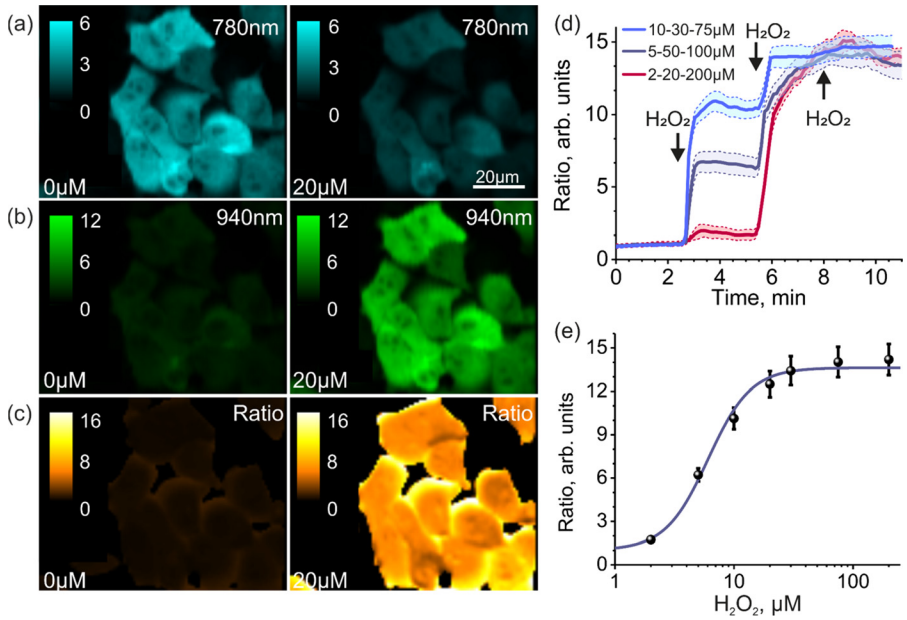

FIG. 5. (a)–(c) 2PEF images of HeLa cells with HyPer7 under excitation at 780 nm (a) and 940 nm (b), and the ratiometric images (c) before (left column) and after (right column) addition of the saturation H_2O_2 concentration 20 μM. (d) Dynamics of the ratio signals of HyPer7, which reflect H_2O_2 dynamics changes in HeLa cells when H_2O_2 was added (black arrows) to the medium at concentrations of 2–20–200 μM (red line), 5–50–100 μM (navy line), and 10–30–75 μM (blue line). (e) The dependence of HyPer7 signal in HeLa cells on H_2O_2 concentration in the medium. The Hill's function fit is shown by the navy line.

proteins in their different functional forms [Figs. 4(c)–4(h)]. The common feature of the all TPA spectra is a pronounced peak at the wavelength of 950 nm, not coinciding with the doubled value of the OPA maximum at ~500 nm, which is explained by the vibration-assisted optical transmission between the background and the first electronic excited states.[20] All these proteins show significant differences in the TPA profiles in their maximum states, which provides great potential for ratio signal measurements. Defining the dynamic range (DR) of the ratiometric response as $\Re \equiv R_o/R_r$, where $R = \varphi\sigma_2(\lambda_o)/\varphi\sigma_2(\lambda_r)$ yielded at $\lambda_o \approx 940$ nm and $\lambda_r \approx 780$ nm, we could calculate it for the proteins HyPer7, HyPer3, Grx1-roGFP2, RexYFP, Hypocrates, and SypHer3s, resulting in $\Re^{TPA} = 5.6$, 7.1, 6.5, 1.7, 2.7 and 194, respectively. These values are close to the DR received for the one-photo excitation case $\Re^{OPA} = 5.1$, 4.3, 4.3, 1.5, 2.3, and 160 for the same GEFIs. Also, the absolute values of $\varphi\sigma_2$ for most sensors exceed 10 GM, corresponding to brightness of the common calcium indicator GCaMP6m.[49] As a result, high brightness, specificity, and sensitivity of the presented sensors enables its high ability to monitor the redox status *in vivo*. It is noteworthy that RexYFP in the single-photon mode is positioned as an intensiometric indicator;[39] however, in the two-photon excitation spectrum, we observe a clear NADH-induced ratiometric response; this fact is an extremely important advantage for *in vivo* studies.

An alternative modality of the optical platform is dual-channel 2PEF microscopy of ratiometric GEFIs. Measurements of the TPA spectra show that all of the present sensors can be efficiently interrogated in a ratiometric manner using radiation having solitary spectral features at 780 and 940 nm. We used the SPM-induced supercontinuum presented in Fig. 3(a) to visualize in real-time the dynamics of hydrogen peroxide in a cell culture, for which they were transfected by the pCS2+ plasmid with HyPer7 gene. The streaming is performed by sequential recording of a 2PEF image pair at the excitation wavelengths of 780 nm [Fig. 5(a)] and 940 nm [Fig. 5(b)], with their ratio providing information on H_2O_2 concentrations [Fig. 5(c)]. During three series of experiments, we added to the cells the buffer with H_2O_2 at concentrations of 2–20–200, 10–50–75, and 100–200–300 μM in individual Petri dishes. Each series was repeated three times. In Fig. 5(c), we show that the ratiometric 2PEF microscopy allows us to analyze the temporal dynamics of H_2O_2 concentration changes in individual cells' compartments and the cell ensemble. The ratiometric nature of the HyPer7 response provides quantitative data independently on the cellular level of the sensor.[27] By changing the H_2O_2 concentrations, we were able to titrate the nonlinear HyPer7 ratio response R and approximate the experimental values with the Hill's function $R = R_m/(1 + (K_a/C[H_2O_2])^n)$, where $R_m = 13.6 \pm 0.8$, $K_a = 6.0 \pm 0.6$ μM, and $n = 2.4 \pm 0.3$ [Fig. 5(e)]. Saturation of the ratio is exceeded with extracellular H_2O_2 density of about $\sim 2K_a = 12$ μM, and the full dynamic range R_m is about 14, which closely aligns with values obtained through ratiometric 1PE at the wavelengths of 490 and 405 nm.[38]

To summarize, we propose a design for a cheap and compact hybrid spectroscopic-imaging PCF-based setup for investigating ratiometric fluorescent indicators' ability to image biological systems by two-photon microscopy. We obtained quantitative two-photon absorption spectra of the popular GEFIs having high sensitivity and one-photon brightness. We have shown that accurate control under nonlinear transformation of ultrashort pulses in PCF combined with spectrum management, including amplitude and phase steering, could provide an appropriate laser source for the selection and 2PEF imaging of ratiometric fluorescent sensors. The long-term stability of the source is demonstrated by the ability to record the temporal dynamics of the ratiometric HyPer7 probe response in cells for tens of minutes.

See the supplementary material for more information about the PCF-based laser source.

The authors are grateful to professor A. M. Zheltikov for comprehensive support. The ultrashort pulse optimization and TPA

spectra measurements were supported by Grant Nos. 22-12-00149 and 22-72-10044 of the Russian Science Foundation (RSF). The biological part of the work was supported by the RSF with Grant No. 23-75-30023.

AUTHOR DECLARATIONS

Conflict of Interest

The authors have no conflicts to disclose.

Author Contributions

Artem S. Chebotarev: Data curation (lead); Formal analysis (lead); Investigation (equal); Software (equal). **Roman I. Raevskii:** Data curation (equal); Investigation (equal); Resources (equal). **Georgy N. Linovsky:** Data curation (supporting); Formal analysis (equal); Software (equal). **Alexander I. Kostyuk:** Methodology (equal); Resources (equal). **Vsevolod V. Belousov:** Funding acquisition (equal); Resources (equal); Supervision (supporting). **Andrei B. Fedotov:** Funding acquisition (equal); Methodology (supporting); Resources (equal); Supervision (supporting). **Dmitry S. Bilan:** Conceptualization (equal); Resources (supporting); Supervision (supporting); Writing – review & editing (equal). **Aleksandr A. Lanin:** Conceptualization (equal); Formal analysis (supporting); Funding acquisition (equal); Methodology (equal); Supervision (equal); Writing – original draft (lead); Writing – review & editing (equal).

DATA AVAILABILITY

The data that support the findings of this study are available from the corresponding author upon reasonable request.

REFERENCES

[1]H. Kamata and H. Hirata, "Redox regulation of cellular signalling," Cell. Signalling **11**, 1–14 (1999).
[2]S. Parvez, M. J. C. Long, J. R. Poganik, and Y. Aye, "Redox signaling by reactive electrophiles and oxidants," Chem. Rev. **118**, 8798–8888 (2018).
[3]H. Sies, V. V. Belousov, N. S. Chandel, M. J. Davies, D. P. Jones, G. E. Mann, M. P. Murphy, M. Yamamoto, and C. Winterbourn, "Defining roles of specific reactive oxygen species (ROS) in cell biology and physiology," Nat. Rev. Mol. Cell Biol. **23**, 499–515 (2022).
[4]J. A. Imlay, "Pathways of oxidative damage," Annu. Rev. Microbiol. **57**, 395–418 (2003).
[5]M. Schieber and N. S. Chandel, "ROS function in redox signaling and oxidative stress," Curr. Biol. **24**, R453–R462 (2014).
[6]H. S. Marinho, C. Real, L. Cyrne, H. Soares, and F. Antunes, "Hydrogen peroxide sensing, signaling and regulation of transcription factors," Redox Biol. **2**, 535–562 (2014).
[7]R. H. Burdon, "Superoxide and hydrogen peroxide in relation to mammalian cell proliferation," Free Radical Biol. Med. **18**, 775–794 (1995).
[8]M. Giorgio, M. Trinei, E. Migliaccio, and P. G. Pelicci, "Hydrogen peroxide: A metabolic by-product or a common mediator of ageing signals?," Nat. Rev. Mol. Cell Biol. **8**, 722–728 (2007).
[9]N. R. Love, Y. Chen, S. Ishibashi, P. Kritsiligkou, R. Lea, Y. Koh, J. L. Gallop, K. Dorey, and E. Amaya, "Amputation-induced reactive oxygen species are required for successful Xenopus tadpole tail regeneration," Nat. Cell Biol. **15**, 222–228 (2013).
[10]A. I. Kostyuk, A. S. Panova, A. D. Kokova, D. A. Kotova, D. I. Maltsev, O. V. Podgorny, V. V. Belousov, and D. S. Bilan, "In vivo imaging with genetically encoded redox biosensors," Int. J. Mol. Sci. **21**, 8164 (2020).
[11]B. Morgan, K. Van Laer, T. N. E. Owusu, D. Ezeriņa, D. Pastor-Flores, P. S. Amponsah, A. Tursch, and T. P. Dick, "Real-time monitoring of basal H_2O_2 levels with peroxiredoxin-based probes," Nat. Chem. Biol. **12**, 437–443 (2016).
[12]D. S. Bilan and V. V. Belousov, "In vivo imaging of hydrogen peroxide with HyPer probes," Antioxid. Redox Signaling **29**, 569–584 (2018).
[13]M. P. Murphy, H. Bayir, V. Belousov, C. J. Chang, K. J. Davies, M. J. Davies, T. P. Dick, T. Finkel, H. J. Forman, and Y. Janssen-Heininger, "Guidelines for measuring reactive oxygen species and oxidative damage in cells and in vivo," Nat. Metab. **4**, 651–662 (2022).
[14]K. C. Wagener, B. Kolbrink, K. Dietrich, K. M. Kizina, L. S. Terwitte, B. Kempkes, G. Bao, and M. Müller, "Redox indicator mice stably expressing genetically encoded neuronal roGFP: Versatile tools to decipher subcellular redox dynamics in neuropathophysiology," Antioxid. Redox Signaling **25**, 41–58 (2016).
[15]M. O. Breckwoldt, F. M. J. Pfister, P. M. Bradley, P. Marinković, P. R. Williams, M. S. Brill, B. Plomer, A. Schmalz, D. K. St Clair, R. Naumann, O. Griesbeck, M. Schwarzländer, L. Godinho, F. M. Bareyre, T. P. Dick, M. Kerschensteiner, and T. Misgeld, "Multiparametric optical analysis of mitochondrial redox signals during neuronal physiology and pathology *in vivo*," Nat. Med. **20**, 555–560 (2014).
[16]A. S. Chebotarev, I. V. Kelmanson, A. D. Ivanova, Y. V. Khramova, V. A. Katrukha, D. A. Kotova, R. I. Raevskii, A. A. Moshchenko, G. N. Linovsky, A. B. Fedotov, V. V. Belousov, D. S. Bilan, and A. A. Lanin, "Multiphoton tools for hydrogen peroxide imaging in vivo with subcellular resolution," Sens. Actuators, B **410**, 135646 (2024).
[17]A. A. Lanin, A. S. Chebotarev, M. S. Pochechuev, I. V. Kelmanson, D. A. Kotova, D. S. Bilan, Y. G. Ermakova, A. B. Fedotov, A. A. Ivanov, V. V. Belousov, and A. M. Zheltikov, "Two- and three-photon absorption cross-section characterization for high-brightness, cell-specific multiphoton fluorescence brain imaging," J. Biophotonics **13**, e201900243 (2020).
[18]A. A. Lanin, M. S. Pochechuev, A. S. Chebotarev, I. V. Kelmanson, D. S. Bilan, D. A. Kotova, V. S. Tarabykin, A. A. Ivanov, A. B. Fedotov, V. V. Belousov, and A. M. Zheltikov, "Cell-specific three-photon-fluorescence brain imaging: Neurons, astrocytes, and gliovascular interfaces," Opt. Lett. **45**, 836–839 (2020).
[19]A. S. Chebotarev, M. S. Pochechuev, A. A. Lanin, I. V. Kelmanson, D. A. Kotova, E. S. Fetisova, A. S. Panova, D. S. Bilan, A. B. Fedotov, V. V. Belousov, and A. M. Zheltikov, "Enhanced-contrast two-photon optogenetic pH sensing and pH-resolved brain imaging," J. Biophotonics **14**, e202000301 (2021).
[20]M. Drobizhev, S. Tillo, N. S. Makarov, T. E. Hughes, and A. Rebane, "Color hues in red fluorescent proteins are due to internal quadratic Stark effect," J. Phys. Chem. B **113**, 12860–12864 (2009).
[21]M. Drobizhev, N. S. Makarov, S. E. Tillo, T. E. Hughes, and A. Rebane, "Two-photon absorption properties of fluorescent proteins," Nat. Methods **8**, 393–399 (2011).
[22]C. R. Stoltzfus, L. M. Barnett, M. Drobizhev, G. Wicks, A. Mikhaylov, T. E. Hughes, and A. Rebane, "Two-photon directed evolution of green fluorescent proteins," Sci. Rep. **5**, 11968 (2015).
[23]A. A. Lanin, A. S. Chebotarev, N. V. Barykina, F. V. Subach, and A. M. Zheltikov, "The whither of bacteriophytochrome-based near-infrared fluorescent proteins: Insights from two-photon absorption spectroscopy," J. Biophotonics **12**, e201800353 (2019).
[24]V. R. Aslopovsky, A. V. Scherbinin, N. N. Kleshchina, and A. V. Bochenkova, "Impact of the protein environment on two-photon absorption cross-sections of the GFP chromophore anion resolved at the XMCQDPT2 level of theory," Int. J. Mol. Sci. **24**, 11266 (2023).
[25]N. S. Makarov, M. Drobizhev, and A. Rebane, "Two-photon absorption standards in the 550–1600 nm excitation wavelength range," Opt. Express **16**, 4029–4047 (2008).
[26]S. de Reguardati, J. Pahapill, A. Mikhailov, Y. Stepanenko, and A. Rebane, "High-accuracy reference standards for two-photon absorption in the 680–1050 nm wavelength range," Opt. Express **24**, 9053–9066 (2016).
[27]J. Weller, K. M. Kizina, K. Can, G. Bao, and M. Müller, "Response properties of the genetically encoded optical H_2O_2 sensor HyPer," Free Radical Biol. Med. **76**, 227–241 (2014).
[28]K. D. Piatkevich, H.-J. Suk, S. B. Kodandaramaiah, F. Yoshida, E. M. DeGennaro, M. Drobizhev, T. E. Hughes, R. Desimone, E. S. Boyden, and V. V. Verkhusha, "Near-infrared fluorescent proteins engineered from bacterial phytochromes in neuroimaging," Biophys. J. **113**, 2299–2309 (2017).
[29]K. Isobe, W. Watanabe, S. Matsunaga, T. Higashi, K. Fukui, and K. Itoh, "Multi-spectral two-photon excited fluorescence microscopy using supercontinuum light source," Jpn. J. Appl. Phys., Part 2 **44**, L167 (2005).

[30]N. G. Horton, K. Wang, D. Kobat, C. G. Clark, F. W. Wise, C. B. Schaffer, and C. Xu, "In vivo three-photon microscopy of subcortical structures within an intact mouse brain," Nat. Photonics **7**, 205–209 (2013).
[31]H. Tu and S. A. Boppart, "Coherent fiber supercontinuum for biophotonics," Laser Photonics Rev. **7**, 628–645 (2013).
[32]S. You, H. Tu, E. J. Chaney, Y. Sun, Y. Zhao, A. J. Bower, Y.-Z. Liu, M. Marjanovic, S. Sinha, and Y. Pu, "Intravital imaging by simultaneous label-free autofluorescence-multiharmonic microscopy," Nat. Commun. **9**, 2125 (2018).
[33]H. Cheng, S. Tong, X. Deng, H. Liu, Y. Du, C. He, P. Qiu, and K. Wang, "Deep-brain 2-photon fluorescence microscopy in vivo excited at the 1700 nm window," Opt. Lett. **44**, 4432–4435 (2019).
[34]S. You, E. J. Chaney, H. Tu, Y. Sun, S. Sinha, and S. A. Boppart, "Label-free deep profiling of the tumor microenvironment," Cancer Res. **81**, 2534–2544 (2021).
[35]K. F. Tehrani, J. Park, E. J. Chaney, H. Tu, and S. A. Boppart, "Nonlinear imaging histopathology: A pipeline to correlate gold-standard hematoxylin and eosin staining with modern nonlinear microscopy," IEEE J. Sel. Top. Quantum Electron. **29**, 6800608 (2023).
[36]L.-T. Chou, Y.-C. Liu, D.-L. Zhong, W.-Z. Lin, H.-H. Hung, C.-J. Chan, Z.-P. Chen, and S.-H. Chia, "Low noise, self-phase-modulation-enabled femtosecond fiber sources tunable in 740–1236 nm for wide two-photon fluorescence microscopy applications," Biomed. Opt. Express **12**, 2888–2901 (2021).
[37]D. S. Bilan, L. Pase, L. Joosen, A. Y. Gorokhovatsky, Y. G. Ermakova, T. W. J. Gadella, C. Grabher, C. Schultz, S. Lukyanov, and V. V. Belousov, "HyPer-3: A genetically encoded H_2O_2 probe with improved performance for ratiometric and fluorescence lifetime imaging," ACS Chem. Biol. **8**, 535–542 (2013).
[38]V. V. Pak, D. Ezeriņa, O. G. Lyublinskaya, B. Pedre, P. A. Tyurin-Kuzmin, N. M. Mishina, M. Thauvin, D. Young, K. Wahni, S. A. Martínez Gache, A. D. Demidovich, Y. G. Ermakova, Y. D. Maslova, A. G. Shokhina, E. Eroglu, D. S. Bilan, I. Bogeski, T. Michel, S. Vriz, J. Messens, and V. V. Belousov, "Ultrasensitive genetically encoded indicator for hydrogen peroxide identifies roles for the oxidant in cell migration and mitochondrial function," Cell Metab. **31**, 642–653.e6 (2020).
[39]D. S. Bilan, M. E. Matlashov, A. Y. Gorokhovatsky, C. Schultz, G. Enikolopov, and V. V. Belousov, "Genetically encoded fluorescent indicator for imaging NAD+/NADH ratio changes in different cellular compartments," Biochim. Biophys. Acta, Gen. Subj. **1840**, 951–957 (2014).
[40]B. Morgan, M. C. Sobotta, and T. P. Dick, "Measuring E_{GSH} and H_2O_2 with roGFP2-based redox probes," Free Radical Biol. Med. **51**, 1943–1951 (2011).
[41]M. Gutscher, A.-L. Pauleau, L. Marty, T. Brach, G. H. Wabnitz, Y. Samstag, A. J. Meyer, and T. P. Dick, "Real-time imaging of the intracellular glutathione redox potential," Nat. Methods **5**, 553–559 (2008).
[42]A. I. Kostyuk, M.-A. Tossounian, A. S. Panova, M. Thauvin, R. I. Raevskii, D. Ezeriņa, K. Wahni, I. Van Molle, A. D. Sergeeva, and D. Vertommen, "Hypocrates is a genetically encoded fluorescent biosensor for (pseudo) hypohalous acids and their derivatives," Nat. Commun. **13**, 171 (2022).
[43]Y. G. Ermakova, V. V. Pak, Y. A. Bogdanova, A. A. Kotlobay, I. V. Yampolsky, A. G. Shokhina, A. S. Panova, R. A. Marygin, D. B. Staroverov, and D. S. Bilan, "SypHer3s: A genetically encoded fluorescent ratiometric probe with enhanced brightness and an improved dynamic range," Chem. Commun. **54**, 2898–2901 (2018).
[44]A. S. Chebotarev, A. A. Lanin, R. I. Raevskii, A. I. Kostyuk, D. D. Smolyarova, D. S. Bilan, I. V. Savitskii, A. B. Fedotov, V. V. Belousov, and A. M. Zheltikov, "Single-beam dual-color alternate-pathway two-photon spectroscopy: Toward an optical toolbox for redox biology," J. Raman Spectrosc. **52**, 1552–1560 (2021).
[45]J. Shin, W. Cho, K. Yeom, and K. T. Kim, "Tailoring octave-spanning ultrashort laser pulses using multiple prisms," Opt. Express **31**, 22855–22862 (2023).
[46]M. Miranda, T. Fordell, C. Arnold, A. L'Huillier, and H. Crespo, "Simultaneous compression and characterization of ultrashort laser pulses using chirped mirrors and glass wedges," Opt. Express **20**, 688–697 (2012).
[47]B. Alonso, Í. J. Sola, and H. Crespo, "Self-calibrating d-scan: Measuring ultrashort laser pulses on-target using an arbitrary pulse compressor," Sci. Rep. **8**, 3264 (2018).
[48]S. Kane, J. Squier, J. V. Rudd, and G. Mourou, "Hybrid grating–prism stretcher–compressor system with cubic phase and wavelength tunability and decreased alignment sensitivity," Opt. Lett. **19**, 1876–1878 (1994).
[49]L. M. Barnett, T. E. Hughes, and M. Drobizhev, "Deciphering the molecular mechanism responsible for GCaMP6m's Ca^{2+}-dependent change in fluorescence," PLoS One **12**, e0170934 (2017).